esteem3

Enabling Science through European Electron Microscopy

Second report on TEM methods applied to materials for health

Deliverable D9.3 – version 0.3

Estimated delivery date: 31.12.2022

Actual delivery date: 21.12.2022

Lead beneficiary: ANT

Person responsible: Sara Bals

Deliverable type: ☒ R ☐ DEM ☐ DEC ☐ OTHER ☐ ETHICS ☐ ORDP

Dissemination level: ☒ PU ☐ CO ☐ EU-RES ☐ EU-CON ☐ EU-SEC

THIS PROJECT HAS RECEIVED FUNDING FROM THE EUROPEAN UNION'S HORIZON 2020 RESEARCH AND INNOVATION PROGRAMME UNDER GRANT AGREEMENT NO **823717**

Grant Agreement No:	823802
Funding Instrument:	Research and Innovation Actions (RIA)
Funded under:	H2020-INFRAIA-2018-1: Integrating Activities for Advanced Communities
Starting date:	01.01.2019
Duration:	54 months

Table of contents

Revision history log

Version number	Date of release	Author	Summary of changes
V0.1	19/12/2022	Sara Bals Jo Verbeeck	First draft
V0.2	19/12/2022	Peter A. van Aken	Approval
V0.3	20/12/2022	Lucie Guilloteau	Final proofreading

Executive Summary

This report summarises projects performed in STU, ANT and Nano within WP9 – Materials for Health. Five different projects from ANT and two from STU will be discussed. At ANT, there has been a large focus on the development and application of novel low electron dose imaging techniques, since materials with impact in the broad field of health are often very sensitive to the electron beam (Task 1). As an example, we discuss the application of such methods to the investigation of metal-organic frameworks (MOFs), which are known to be of great use for controlled drug delivery (Task 2). In deliverable 9.2, we already reported on the investigation of anisotropic Au nanoparticles, which can e.g. be used during biosensing or for photothermal ablation of cancer cells. Here, we performed electron tomography investigations of hybrid nanoparticles comprising an iron oxide core and an outer gold spiky layer, stabilized by a biocompatible polymeric shell. The combined magnetic and optical properties of the different components provide the required functionalities for magnetic resonance imaging (MRI), surface-enhanced Raman scattering (SERS), and fluorescence imaging (Task 3). To assess the thermal stability of metallic nanoparticles used in the field of health, *in situ* heating investigations using electron tomography are of high importance. Following up on previous work, we investigated AuPt bimetallic nanoparticles, which have been considered in literature for use in in immunoassays or as antibacterials (Task 4). Finally, ANT and Nano have collaborated to extend the 3D investigation of such plasmonic Au nanoparticles to a 3D characterization in a liquid environment using dedicated liquid cells (Task 5). Such studies are of crucial to understand the behaviour of the metal nanoparticles in biological cells, in which they eventually are to be applied. In STU the focus has been on optimization and development of sample preparation techniques that can be applied for preparation of organic/inorganic materials important for health. New protocols have been developed and will be published on ESTEEM3 webpage after manuscripts will be accepted for publication. In addition, all prepared samples are being characterized in detail by using imaging and spectroscopic methods.

Task 1: Dose-efficient methods for electron beam sensitive materials (ANT)

Beam damage is by far the most important aspect that hampers the use of electron microscopy for organic materials and many materials with applications in the field of health. Consequently, information obtained for such samples is much less reliable and yields significantly lower resolution compared to typical crystalline inorganic samples. Several low-dose imaging methods are being developed in the ESTEEM3 project that aim to overcome these limitations. In this report, we will discuss the underlying developments and the application for samples relevant to the domain of health. Our ultimate goal is to apply the low-dose imaging techniques to biological materials. However, as a proof of principle, we will here focus on high-resolution imaging of inorganic, but extremely beam sensitive materials. In task 2, we will apply the most promising techniques to MOFs, which are of great importance for health applications, since they can be used as drug carriers.

Many state-of-the-art detectors, based on hybrid-detector technology (e.g. Timepix), focus on lower pixel count together with higher readout speeds and beam hardness. This makes them suitable for so-called 4D-Scanning Transmission Electron Microscopy (4D-STEM), a technique based on a STEM probe scanned setup. For every probe position, individual diffraction patterns are recorded. Consequently, such 4D datasets contain -all- scattering information about the sample and not a single electron is discarded. Because of the efficient use of all electrons, 4D STEM holds high potential for imaging beam sensitive samples. Compared to conventional TEM imaging, which is still the most popular imaging method for life science, 4D STEM could reveal more contrast and result in more information per incoming electron. Until recently, the application of 4D STEM to beam sensitive samples was hampered by low scan speeds, but since this problem has been solved [1], the current main challenge is to develop methods to extract and represent the information that is encoded in the large 4D STEM datasets.

Different approaches are being developed by ANT, involving standard ptychographic reconstruction algorithms [2], real-time integrated centre of mass (riCOM) [3] and artificial intelligence variations of ptychographic reconstruction [4]. The current state-of-the-art has reached a level, where one can now perform real time imaging with 4D STEM providing high contrast images from dose levels that were unachievable at the start of the ESTEEM3 project. A comparison of different imaging techniques is presented in Figure 1 for a zeolite material, known for its extreme beam sensitivity and used as a proof-of-concept in this deliverable.

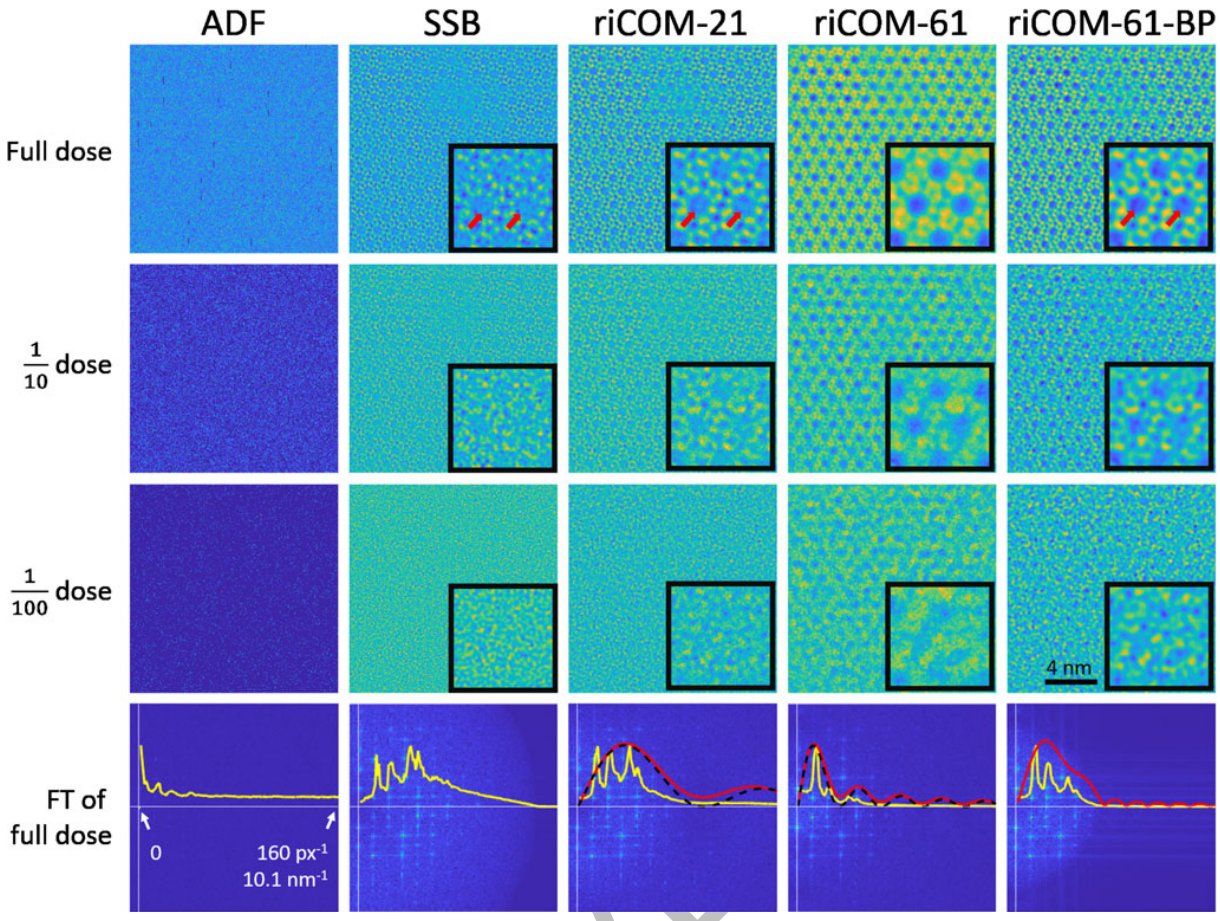

Figure 1: Reconstructed image from an experimental zeolite dataset with different doses (full dose: 1.27 $10^4 e^-/Å^2$). Annular Dark Field (ADF) images are generated by integrating the intensities in the detector area beyond the convergence angle at each probe position. For Single Side Band (SSB) reconstruction (based on the concept of ptychography), a frame-based dataset is first generated from the event array, with the detector space binned down to 32 × 32 (eight times smaller). For riCOM reconstruction, three different kernels are used: 21×21, 61×61, and 61×61 with a band-pass filter. The effect is, however, much less significant in other reconstruction methods. The insets show magnified versions of the centre of their respective images, and the red arrows point out intensity fluctuations within the holes. The last row shows the Fourier transform of each reconstructed result. The radial averaged frequency spectra are represented with yellow curves, the frequency components of each kernel in red, and the line-integration approximation in a black dashed curve [3].

Another research line focuses on changing the way samples are scanned. Indeed, going beyond conventional raster like scanning was demonstrated to result in a significant lowering of the beam damage without changing the total electron dose [5]. Even though the full physical understanding of this effect is still an ongoing topic of research [6], the fact that beam damage could be reduced while maintaining the total electron dose could be considered a revolution for life science imaging. We again used a zeolite material as a proof-of-principle and the results are presented in Figure 2

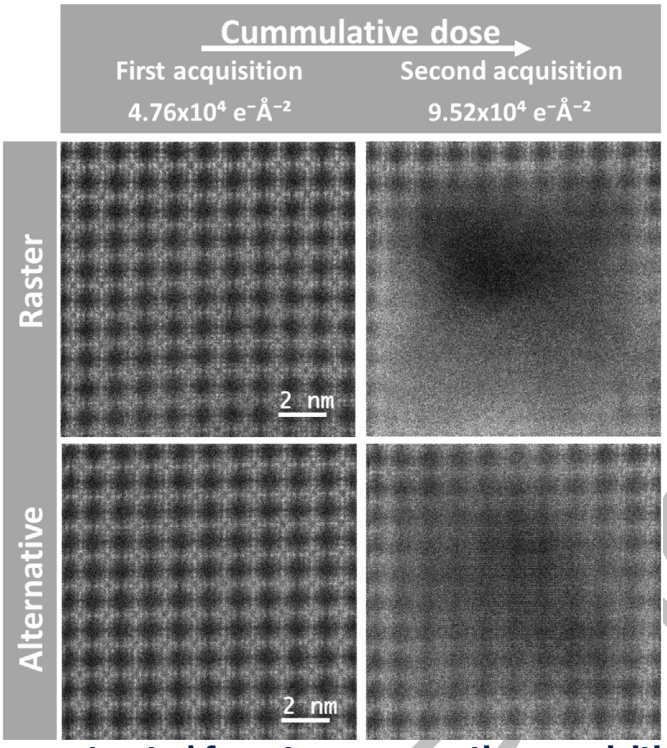

Figure 2: Sub-images extracted from two consecutive acquisitions over the same 3 × 3 sub-images experiment. The scanning was performed with 24.3 pm pixel size, 9 µs dwell time and a calculated dose of approximately 4.76 × 10^4 $e^-/Å^2$ per acquisition. The contrast on the raw images is chosen equal to allow a fair comparison of the evolution under beam damage [5].

Task 2: Imaging metal-organic frameworks for controlled drug delivery (ANT)

MOFs are both porous and crystalline materials that consist of metal nodes and organic linkers. Amongst the many potential applications, MOFs are of great interest as nanocarriers for controlled drug release. Nanocomposites, consisting of inorganic nanoparticles surrounded by a MOF shell, can promote drug delivery under a specific stimulus. Hereby, the use of plasmonic nanoparticles (see Task 3 and Deliverable 9.2) allows the heating of such nanocomposites by near-infrared (near-IR) illumination in a controlled manner, triggering a localized drug release from the pores of the MOF. Understanding these mechanisms is of great interest, but unfortunately, MOFs are very quickly destroyed under electron irradiation. This beam sensitivity is especially critical when performing electron tomography measurements, where multiple images of a single particle are collected to obtain a 3D characterization. We have therefore applied the riCOM approach developed in Task 1 to the investigation of MOFs.

In Figure 3, we first compare the use of high angle annular dark field STEM (HAADF-STEM) and differential phase contrast (iDPC), which is considered as the state-of-the-art to image MOFs at high resolution. This comparison, for the MIL-101 structure indeed shows that iDPC results in images with significantly improved information transfer from 8 Å to 3.3Å.

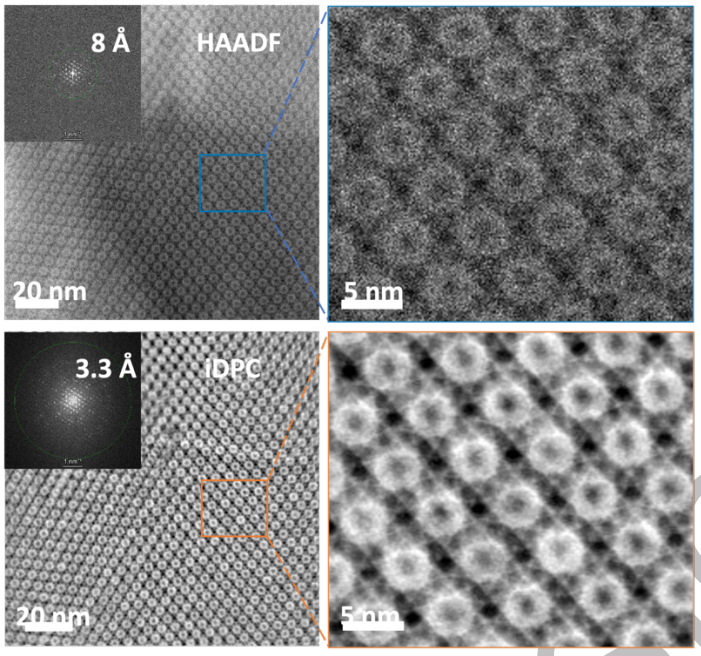

Figure 3: HAADF and iDPC images of MIL-101, imaged along the (110) zone axis, and acquired simultaneously. Top left insets show the FFT of corresponding images with their information transfer values. Images were acquired with an electron dose of 114.67 $e^-/Å^2$.

Although iDPC images are very valuable to characterize MOFs, the possibility of obtaining immediate feedback while imaging by riCOM has large benefits for the investigation of beam sensitive materials. We therefore also applied this technique to the MIL-101 crystals, as illustrated in Figure 4. At very low dose, high-resolution information can be extracted and it is of great importance to note that the organic linkers can be detected. Clearly, this approach holds great promise to further investigate nanoparticle-MOF composites without electron beam damage. In future experiments, this will enable us to investigate the effect of heat or light on the drug release mechanisms without a degrading influence of the electron beam.

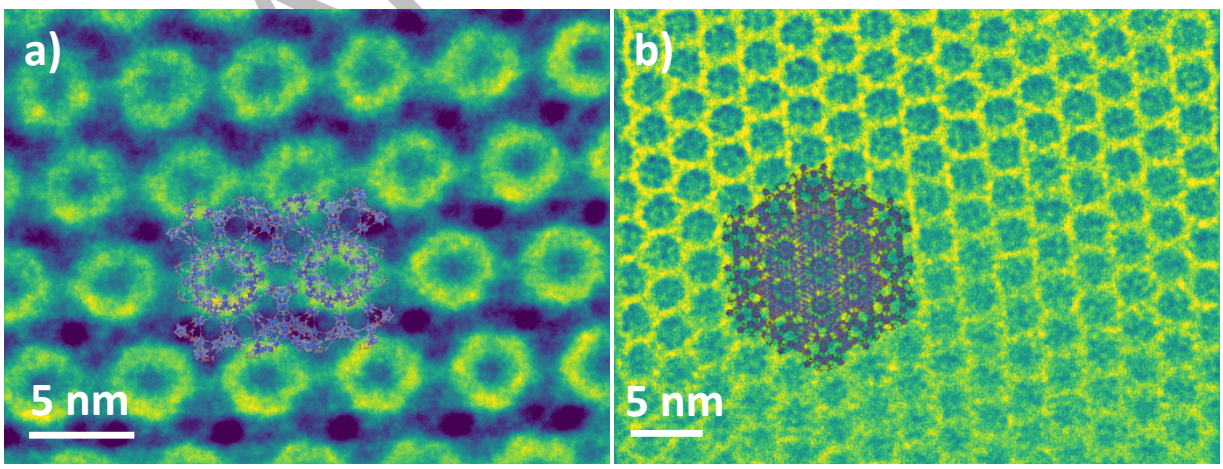

Figure 4: riCOM images of MIL-101 imaged along a) (110), and b) (111) zone axes, respectively. Images were acquired with an electron dose of 8.9, and 1.12 $e^-/Å^2$, respectively. Expected crystal structures are superimposed on the images and an excellent match is observed.

Task 3: Electron tomography of hybrid magnetic–plasmonic nanoparticles (ANT)

The anisotropic and pointed nature of Au nanostars (AuNSs) has been shown to render them excellent Raman enhancers because of the particularly efficient electromagnetic field enhancement. However, the diamagnetic nature of gold does not make it useful for more common nuclear magnetic resonance (NMR)-based techniques, most often used for whole-body imaging in clinical settings. Therefore, many attempts have been made toward combining Au with magnetic NPs, namely iron oxide NPs (IONPs), to conduct simultaneous imaging by MRI, CT, and SERS. A 3D reconstruction is therefore of great importance.

To obtain quantitative information about the thickness and structure of gold shells (e.g., number of spikes) covering the iron-oxide cores, a detailed characterization by electron microscopy and electron tomography was carried out. Such an analysis is important to evaluate the surface area. A representative 3D visualization of the hybrid structures retrieved by HAADF-STEM tomography is shown in Figure 5. Using a manual segmentation process and a surface generation module, boundary surfaces were extracted for Au surface area determination. More detailed information can be found in [7].

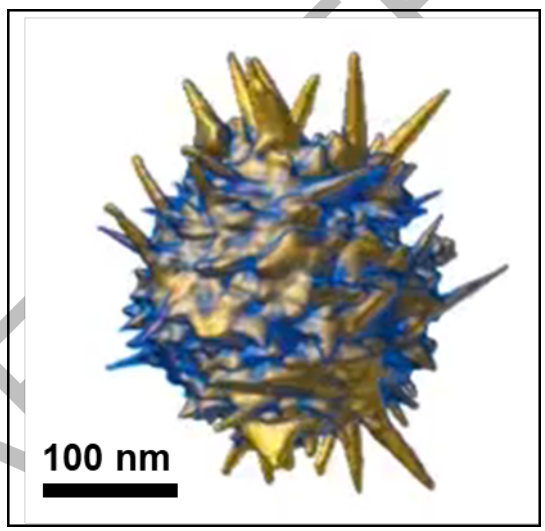

Figure 5: 3D reconstruction of the hybrid iron oxide (blue) - gold (yellow) nanoparticles, obtained by HAADF-STEM tomography.

Task 4: Thermal stability of bimetallic nanoparticles (ANT)

Anisotropic Au nanoparticles are of great interest in the field of medicine, since their plasmonic properties can be exploited during e.g. photothermal ablation of cancer cells. These properties are strongly dependent on the morphology and 3D structure of such nanoparticles. In deliverable 9.2, we also investigated morphological and compositional transformations of (bi)metallic AgAu nanoparticles. Here, we present a 3D investigation of AuPt nanoparticles, which

have been proposed in literature for their use of antibacterials [8]. Unfortunately, these materials are thermally very unstable. To investigate the thermal instability of AuPt nanorods at temperatures below their bulk melting point, we combined *in situ* heating with 2D and 3D electron microscopy techniques, including 3D energy-dispersive X-ray spectroscopy [9].

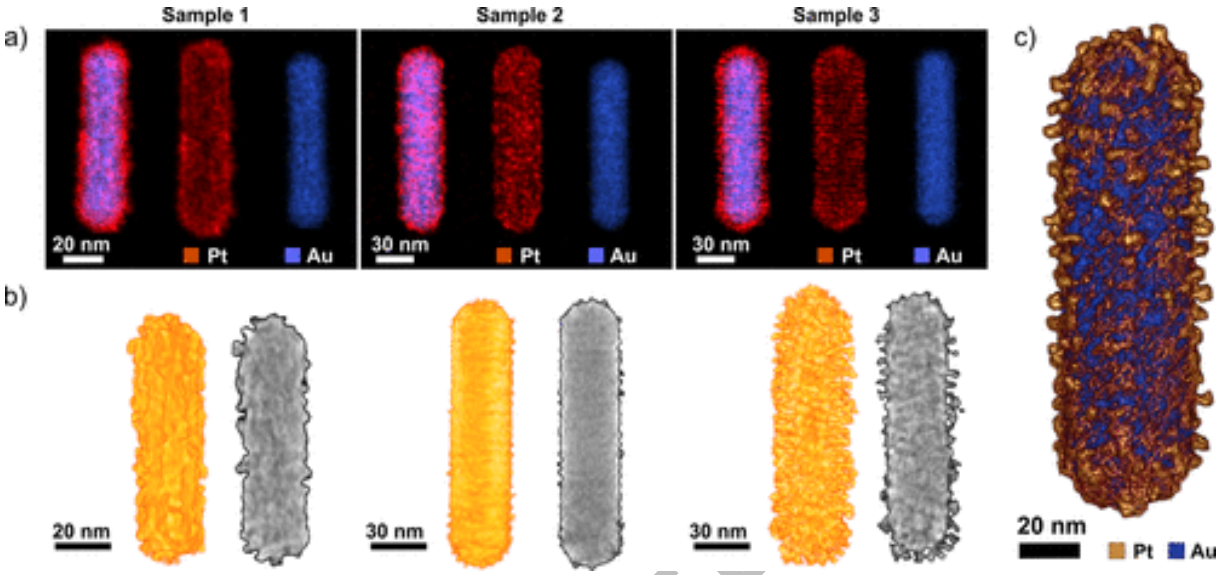

Figure 6: (a) EDX-STEM maps of Au@Pt NR samples (1), (2) and (3), with different [Pt/Au]; molar ratios calculated from EDX-STEM data are 0.8, 0.1 and 0.3, respectively. (b) 3D visualizations and orthoslices through the 3D HAADF-STEM reconstructions. (c) 3D visualization of the EDX-STEM tomography reconstruction obtained from a representative sample [9].

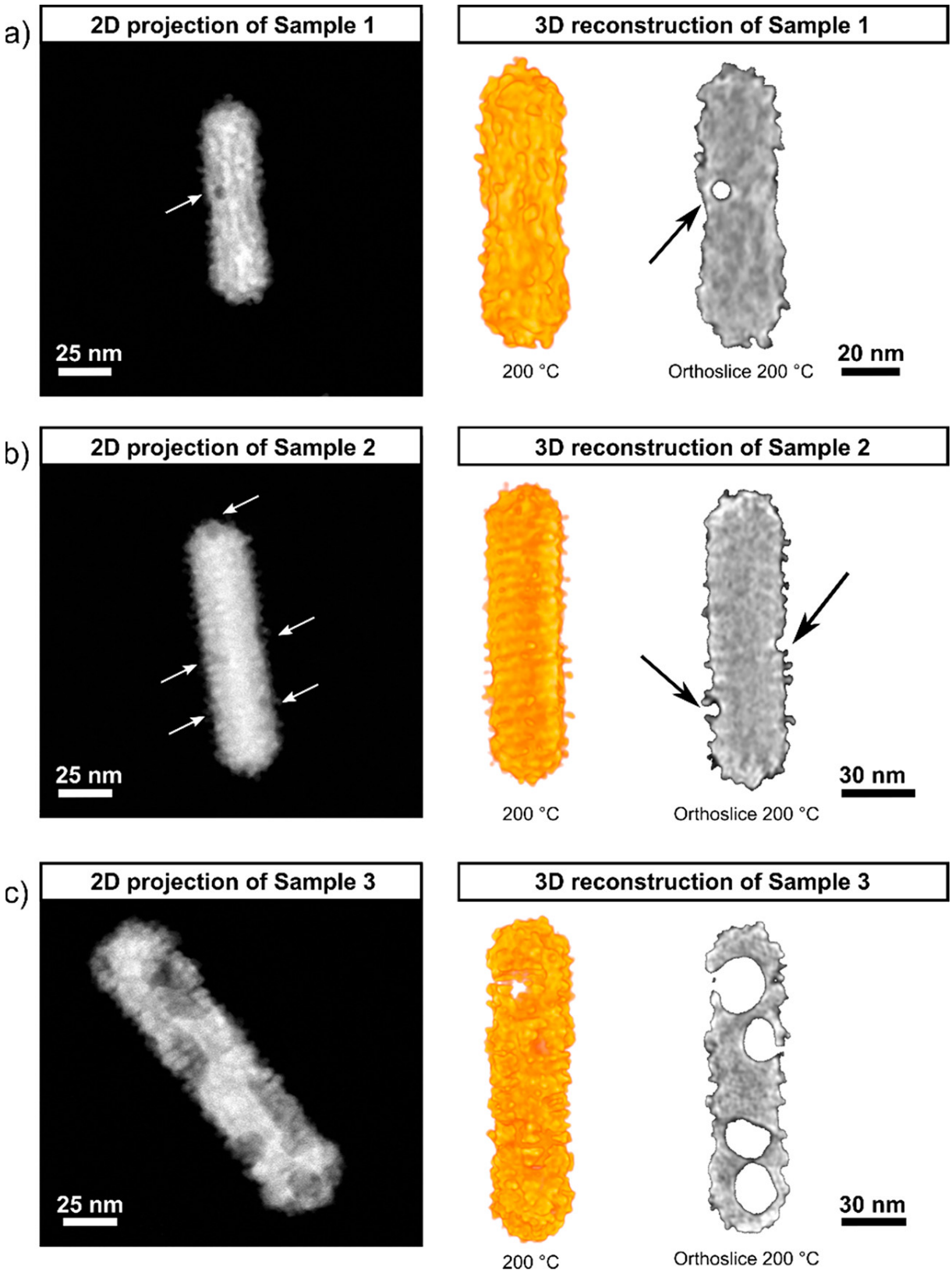

Figure 7: In situ heating tomography experiments. 2D projections, 3D visualizations, and selected orthoslices through the HAADF-STEM reconstructions obtained for the selected samples (as labeled), after heating at 200 °C for 5 min. Small voids and indentations observed in samples (1) and (2) are marked in the 2D projection images by white arrows and by black arrows in the orthoslices [9].

The experimental results were used as input for molecular dynamics simulations, to unravel the mechanisms behind the morphological transformation of AuPt core–shell nanorods. We conclude that thermal stability is influenced not only by the degree of coverage of Pt on Au but also by structural details of the Pt shell. Figure 6 shows the different samples that have been investigated, whereas Figure 7 illustrates the observed thermal instability. By using the outcome of the electron tomography investigations as input for molecular dynamics simulations, we were able to determine the optimal configuration of the Pt shell to enhance the thermal stability (Table 1).

Table 1: Percentage of diffused Au atoms after heating at 200 °C by MD simulations for Au@Pt NRs with different Pt surface coverage and thickness of the Pt shell.

Thickness of Pt shell	Surface Coverage of Pt Shell →									
	44.5%	50.8%	54.6%	57.8%	65.3%	74.1%	82.1%	83.9%	89.0%	100%
2 atom-thick	4.9 %	6.4 %	7.2 %	8.1 %	9.7 %	9.8 %	9.2 %	7.6	3.3	2.0 %
3 atom-thick	5.1 %	6.6 %	7.2 %	8.1 %	9.7 %	7.3 %	5.6%	3.4	2.0	0.5 %
4 atom-thick	5.1 %	6.5 %	7.4 %	8.5 %	9.6 %	6.3 %	5.4%	3.8	2.2	0.0 %
5 atom-thick	5.3 %	6.8 %	7.8 %	8.9 %	9.8 %	6.2 %	5.5 %	4.1 %	2.3 %	0.0 %

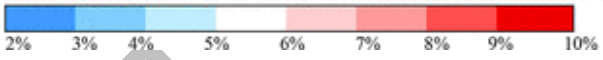

Task 5: 3D investigation of plasmonic nanoparticles in a liquid environment (ANT&NANO)

A current disadvantage of (S)TEM in 2D and 3D, within the framework of the investigation of materials for health, is the need for high vacuum, so conventional (S)TEM imaging of nanoparticles and assemblies, as well as their interaction with surface ligands, proteins and macromolecules, may not reflect their actual appearance in a liquid or a biofluid. To investigate nanoparticles in a liquid environment, dedicated holders are available, but the tilt range is too limited for electron tomography. Recently, Nanomegas developed prototype Tomochips (Figure 8) that enable a tilt range large enough for 3D imaging [10].

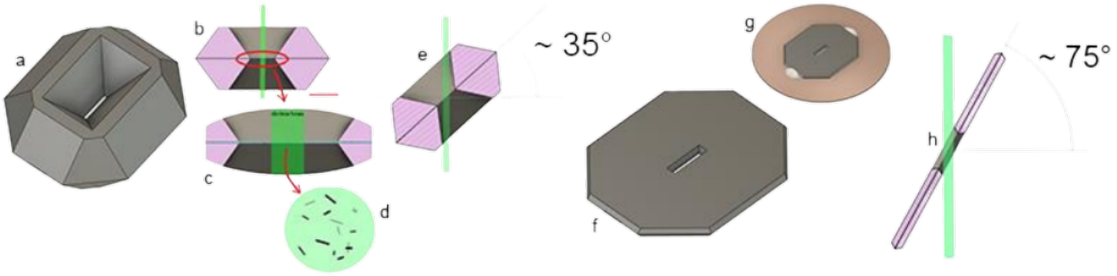

Figure 8: Conventional liquid cells (left) with limited tilt range, compared to dedicated tomo liquid cells, enabling a tilt range for tomography.

Preliminary results for a Au assembly of nanorods are presented in Figure 9, it can be seen that the interparticle distance is different for the dried and liquid state. These possibilities will be of great impact to understand the behaviour of nanoparticles, used for health applications in a relevant environment.

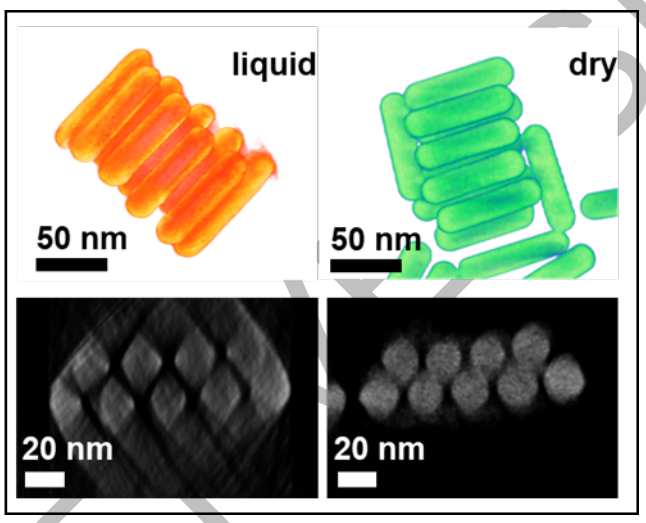

Figure 9: 3D reconstructions of an assembly of nanoparticles. Tilt series for tomography were acquired in dried state (left) and using dedicated liquid tomo chips (left). 3D visualisations (top) and orthoslices (bottom) are presented

Task 6: Advanced sample preparation and characterization of organic/inorganic materials (STU)

Composite organic/inorganic materials are highly challenging in terms of sample preparation and TEM investigations due to different physical, chemical and mechanical properties of their constituent elements. Different polishing and milling rates represent a serious limitation that needs to be overcome. With the latest developments of modern electron microscopes, the quality of TEM samples is often a limiting factor for successful investigations.

During the ultramicrotomy (UM) preparation of natural organic/inorganic materials, their composition could be altered due to de-mineralization processes

while electron transparent slices are floating on the water. To study if such processes effect also our materials, we have compared samples that were prepared by different methods. We have optimized the preparation of electron-transparent slices from dentine areas in rodent teeth by UM (Figure 10) and a combination of UM, focused ion beam (FIB) and Nano-mill (NM) ion milling techniques (Figure 11).

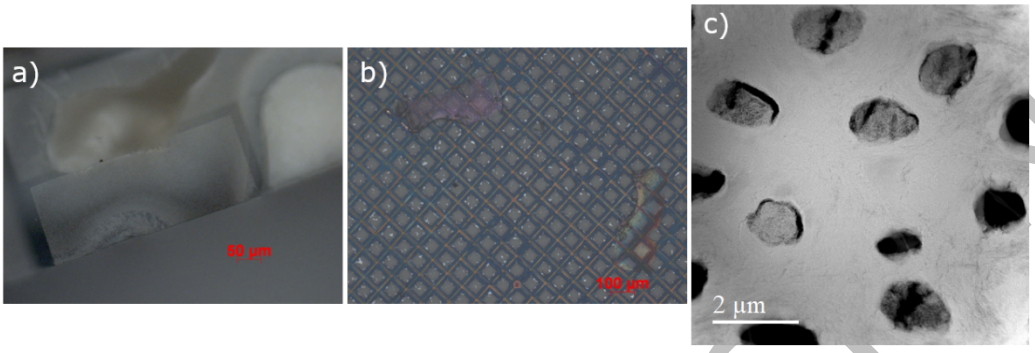

Figure 10: Ultramicrotomy sample preparation of rodent dentine. (a) Block face, (b) electron-transparent slices deposited on a Cu grid, and (c) dentinal tubules in dentine.

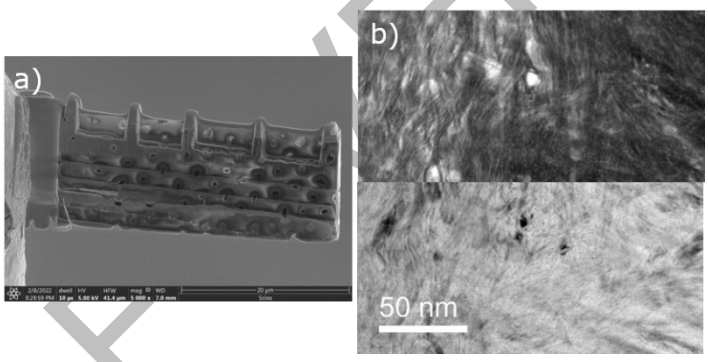

Figure 11: Sample preparation of rodent dentine by a combination of UM, FIB and NM. (a) SEM, (b) BF-STEM (top) and HAADF-STEM (bottom) images.

Table 2: Samples of rodent dentine prepared by UM and combination of UM+FIB+NM characterized by EDX. Quantification was done by using experimentally determined k-factors.

DENTIN (D)	UM	UM+FIB+NM
Mg (at%)	5.4 ± 0.3	4.8 ± 0.2
P (at%)	31.3 ± 1.6	37.1 ± 1.9
Ca (at%)	58.3 ± 2.9	58.1 ± 2.9

All samples have been characterized by a combination of bright-field (BF-) and high-angle annular dark-field (HAADF-) scanning TEM (STEM) imaging and energy-dispersive X-ray spectroscopy (EDX, Table 1). We have experimentally determined k-factors that were used for the quantitative characterization of the dentine composition. There are only minor variations in composition when comparing samples prepared by UM and UM+FIB+NM, that could be also attributed to compositional variations in material. Based on these results we can conclude that samples prepared by UM were not affected by the sample preparation and can be used for our further measurements [11].

In another study, the interplay of the mineral distribution and the orientation of the organic matrix was studied in the claws of the sea slater. We determined the structural and compositional features of claws (Figure 12). Backscattered electron imaging (BSE) together with EDX elemental mapping using a scanning electron microscope (SEM) enabled us to determine the distribution of mineral components in the cuticule. In the claws, the concentration of calcium (Ca) and phosphorous (P) is high in the inner layers of the cuticule. The relatively thick outer layers show elevated amounts of bromine (Br). HAADF-STEM imaging of samples prepared by UM allowed us to determine the organization of organic and mineral components of the cuticule at the nanometer scale. We found the presence of amorphous calcium phosphate in the endocuticule and non-mineralized exocuticule with elevated amounts of Br (Figure 13) [12].

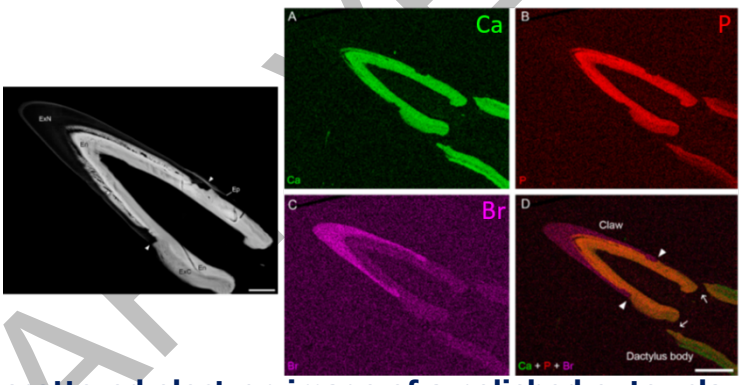

Figure 12: Backscattered electron image of a polished outer claw in longitudinal section with corresponding Ca, P, Br maps obtained by EDX.

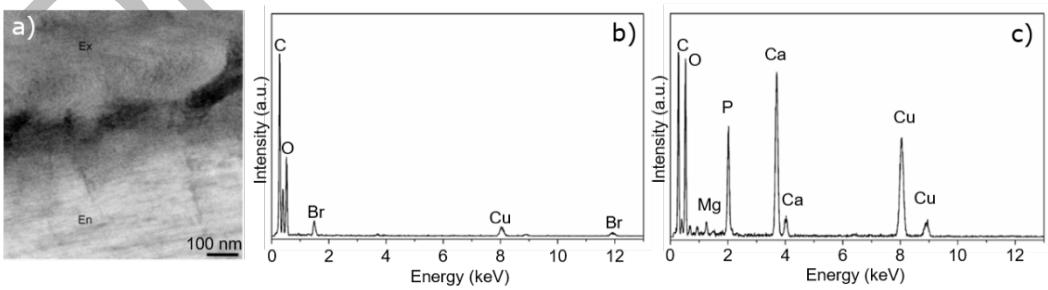

Figure 13: (a) HAADF-STEM image of the cuticule at the base of the outer claw with corresponding EDX spectra measured from the non-mineralized claw exocuticule (b) and claw endocuticule.

References:

1. "*Event driven 4D STEM acquisition with a Timepix3 detector: Microsecond dwell time and faster scans for high precision and low dose applications*". Jannis D, Hofer C, Gao C, Xie X, Béché A, Pennycook Tj, Verbeeck J, Ultramicroscopy **233**, 113423 (2022).

2. "*Overcoming contrast reversals in focused probe ptychography of thick materials: An optimal pipeline for efficiently determining local atomic structure in materials science*". Gao C, Hofer C, Jannis D, Béché A, Verbeeck J, Pennycook TJ, Applied Physics Letters **121**, 081906 (2022).

3. "*Real-Time Integration Center of Mass (riCOM) Reconstruction for 4D STEM*". Yu C-P, Friedrich T, Jannis D, Van Aert S, Verbeeck J, Microscopy And Microanalysis , 1 (2022).

4. *"Phase Object Reconstruction for 4D-STEM using Deep Learning"* . Friedrich T, Yu C-P, Verbeeck J, Van Aert S, arXiv:2202.12611.

5. "*Reducing electron beam damage through alternative STEM scanning strategies, Part I: Experimental findings*". Velazco A, Béché A, Jannis D, Verbeeck J, Ultramicroscopy **232**, 113398 (2022).

6. "*Reducing electron beam damage through alternative STEM scanning strategies, Part II: Attempt towards an empirical model describing the damage process*". Jannis D, Velazco A, Béché A, Verbeeck J, Ultramicroscopy , 113568 (2022).

7. "*Hybrid Magnetic–Plasmonic Nanoparticle Probes for Multimodal Bioimaging*". de la Encarnación C, Lenzi E, Henriksen-Lacey M, Molina B, Jenkinson K, Herrero A, Colás L, Ramos-Cabrer P, Toro-Mendoza J, Orue I, Langer J, Bals S, Jimenez de Aberasturi D, Liz-Marzán LM, The Journal of Physical Chemistry C **126** 19519-19531 (2022).

8. "Tuning the composition of AuPt bimetallic nanoparticles for antibacterial application". Zhao Y, Ye C, Liu W, Chen R, Jiang X, Angew. Chem., Int. Ed. **53** 8127-8121 (2014).

9. "*Thermal Activation of Gold Atom Diffusion in Au@Pt Nanorods*". Pedrazo-Tardajos A, Arslan Irmak E, Kumar V, Sánchez-Iglesias A, Chen Q, Wirix M, Freitag B, Albrecht W, Van Aert S, Liz-Marzán LM, Bals S, ACS Nano **16** 9608-9619 (2022).

10. "*High Angle Liquid Cell TEM Tomography for In Situ Observation and 3D Reconstruction in Liquid"*. Partha Pratim Das, Jennifer Cookman, Alejandro Gómez Pérez, Sergi Plana-Ruiz, Miguel López-Haro, José J. Calvino, Jesús Gonzalez Casablanca, Evangelos Grivas, Georgios S.E. Antipas, Nikolaos A. Ntallis and Stavros Nicolopoulos; Microscopy and Microanalysis 28(S1) 854-856 DOI: 10.1017/S1431927622003804 (2022)

11. 2 manuscripts in preparation

12. "*The mechanical consequences of the interplay of mineral distribution and organic matrix orientation in the claws of the sea slater ligia pallasii*". Vittori M, Srot V, Korat L, Rejec M, Sedmak P, Bussmann B, Predel F, van Aken PA, Strus J, Minerals **11** 1373 (2021).